National Transportation Safety Board
Office of Research and Engineering
Washington, DC 20594

CEN22FA317

MATERIALS LABORATORY

Factual Report 23-003

February 3, 2023

(This page intentionally left blank)

A. ACCIDENT INFORMATION

Location: Chapelle, New Mexico
Date: July 16, 2022
Time: 19:20 mountain daylight time
01:20 coordinated universal time
Vehicle: Bell UH-1H, N911SZ
Investigator: Matthew Walker, AS-CEN

B. COMPONENTS EXAMINED

Pieces of a starter gear
Pinion gear
Metallic fragments

C. EXAMINATION PARTICIPANTS

Specialist Erik Mueller, Ph.D., P.E.
Office of Research and Engineering, NTSB
Washington, DC

D. DETAILS OF THE EXAMINATION

On July 16, 2022, a Bell UH-1H was substantially damaged when it was involved in an accident near Chapelle, NM. The pilot, two tactical flight observers, and the rescue specialist sustained fatal injuries. Two witnesses reported seeing the helicopter descend rapidly, followed by a large dust plume of dust following its ground impact on rural terrain. The helicopter was retained, and the accessory drive outer-driven bevel gear and adjacent components were sent to the NTSB Materials Laboratory for further examination.

Figures 1 and 2 show the fractured bevel gear as received. The gear exhibited multiple fractured teeth, along with an L-shaped chord-oriented fracture that separated the fractured fragments of the gear. The gear did not exhibit any local deformation adjacent to the fracture surface. The vibroetched markings on the faces of the gear remnants stated the following:

81996ASSY 1-080-310-018 1553
MFG 23715 S/N E6 1553

Figure 3 shows a view of the largest fracture surface on the gear. The fracture surface on the gear consisted of several areas with distinct orientations. The initial fracture parallel to the fractured and liberated tooth measured 0.692, with an initiation area for the fracture about 0.327 inches from the outer surface. The larger chord-oriented

fracture portion through the gear measured 1.844 inches long before turning 90°—this section was 1.420 inches long. The remaining 0.668 inches of the fracture exhibited features consistent with ductile overstress fracture. The total length of this fracture surface was 4.62 inches.

The large crack exhibited crack arrest marks, consistent with crack propagation, later determined to be consistent with fatigue. The large fatigue crack initiated at a smaller fatigue crack, present where a liberated gear tooth remnant had been located. Figure 4 shows the smaller, initial fatigue crack and its initiation region, along with the initiation region of the more prominent secondary fatigue crack.

The initiation of the smaller, initial crack was located along the flank of the missing gear tooth, as illustrated in Figure 5. The opposite tooth, which was still part of the gear, exhibited impact, smearing, and wear damage on the face and flank facing the fractured tooth (lower portion of Figure 4). Figure 6 shows that the initial fatigue crack had initiated at multiple sites, present on the edge with the flank.

The initial fatigue area of the crack served as an initiation region for the larger fatigue crack. Figure 7 shows this area, annotated to show the crack propagation direction and its multiple initiation sites. Figure 8 shows some of the initiation sites, consistent with the undulating morphology of the initial fatigue crack.

The larger fracture surface from the bevel gear was examined using a field emission scanning electron microscope (SEM). Figure 9 shows a typical area on the larger portion of the fatigue crack. Closer views, illustrated sequentially in Figures 10 and 11, demonstrate the fatigue striations present on the surface. The orientation of the striations was consistent with crack propagation from the fractured tooth inward toward the opposite end of the crack.

The small area past the fatigue crack (the final 0.067 inches) exhibited dimpled rupture, consistent with subsequent overstress fracture of the remaining gear cross-section. The fatigue crack's length relative to the gear chord cross-section (~86%) was consistent with relatively low stresses on the gear during crack propagation.

Figure 13 shows a closer view of the initiation sites of the initial crack area at the tooth flank. The edge exhibited smearing damage, indicated by the linear, smooth surface near the edge. There were no indications of corrosion pits or oxide inclusions, but the features present were consistent with wear marks and mechanical damage.

Figure 14 shows the initiation sites of the more prominent secondary fatigue crack. This second set of initiation sites exhibited concentric marks consistent with crack arrest marks oriented inward, consistent with having emanated from the edge (Figure 15). These locations did not reveal material defects such as pits or inclusions. The

features were consistent with geometrical undulations in the lower fatigue crack surface.

Besides the tooth concurrent with the through fracture of the gear, seven other teeth had liberated from the gear. Figure 16 highlights one of the other fractured teeth, exhibiting crack arrest marks similar to that seen early in the large fracture surface. The crack initiation area is located in the middle right of the figure, along the flank toward the inboard side of the tooth valley. Figure 17 shows a different fractured tooth. This fracture exhibited crack arrest marks like the one in Figure 16, along with a second smaller thumbnail crack. This initiation site was also located on a tooth flank toward the outboard corner of the tooth. This fracture also exhibited a secondary crack parallel to the longitudinal tooth direction and consistent with the orientation of the larger fracture surface fatigue crack.

Figure 18 shows the damage to the flank of an adjacent tooth. Oriented longitudinally on the flank, the mark exhibited upward material deformation in the form of smearing. These features were consistent with repeated contact with the mating gear teeth.

The teeth adjacent to the fracture surface were sectioned, mounted in cold epoxy under vacuum, polished, and etched with a 2% Nital solution. Figure 19 shows a tooth in cross-section, showing a generally uniform microstructure, except for the top land. This region exhibited a white layer, which contrasted with the internal microstructure. The core microstructure of the gear exhibited an acicular morphology consistent with a tempered martensitic structure.

Figure 20 shows a closer view of the top land damage, highlighting material deformation. This area exhibited a white color, indicative of untempered martensite. The top land also displayed material with white contrast and acicular dark features, consistent with untempered plate martensite. These features were typical of material being deposited at elevated temperatures (greater than 1300 °F) and rapidly cooled.

Figure 21 shows an adjacent cross-sectioned tooth, which exhibited similar features but with a more pronounced deformed deposit on the top land. This material had been deformed away from the tooth, consistent with the direction opposite that of rotation. Figure 22 shows a closer view, with the tempered microstructure of the tooth core, a surface layer of white untempered martensite, consistent with elevated temperature exposure and rapid cooling, consistent with localized frictional forces. The deposited surface layer exhibited a microstructure similar to the tooth in Figure 20. However, there was also a longitudinal crack along the length of the deformed deposit.

Figure 23 shows a closer view of the flank surface of the tooth cross-section in Figure 19. This flank area did not exhibit any indications of excess high input, showing over

or under-tempering. However, the surface did exhibit minute jagged features, consistent with damage from wearing contact against the faying surfaces of the opposite gear. As shown in the Figure, some of these features had developed into microcracks.

The chemical composition of the gear was examined using EDS and XRF. The composition was consistent with AMS 6260, a low-alloy steel. The hardness was inspected per ASTM E18.[1] The hardness averaged 68 HRA.[2]

The tooth near the largest fatigue fracture was examined using microindentation hardness per ASTM E384.[3] The data were plotted in HRC (converted from HK_{500}) versus the depth from the surface, as illustrated in Figure 24.[4] The amount of data above 50 HRC near the surface was consistent with a case hardening surface treatment. Interpolating the data found the case depth to be consistent with 0.029 inches (0.73 mm) below the surface. This depth was consistent with the drawing requirement to carburizing surfaces to an effective case depth of 0.025 ± 0.005 inches.

Submitted by:

Erik M. Mueller
Materials Research Engineer

---

[1] ASTM E18 – *Standard Test Methods for Rockwell Hardness and Rockwell Superficial Hardness of Metallic Materials*. ASTM International, West Conshohocken, PA.

[2] HRA – Hardness, Rockwell A scale. An indentation method of determining the hardness of metal alloys with an intermediate hardness between the B and C scales, using a conical diamond indenter and 60 kg major load.

[3] ASTM E384 – *Standard Test Method for Knoop and Vickers Hardness of Materials*. ASTM International, West Conshohocken, PA

[4] HK_{500} – an indentation hardness measurement unit obtained by applying a 500-gram load to a Knoop diamond indenter and measuring the size of the resulting impression. Higher numbers indicate harder materials.

HRC – Hardness, Rockwell C scale. An indentation method of determining the hardness of harder metal alloys using a conical diamond indenter and 150 kg major load.

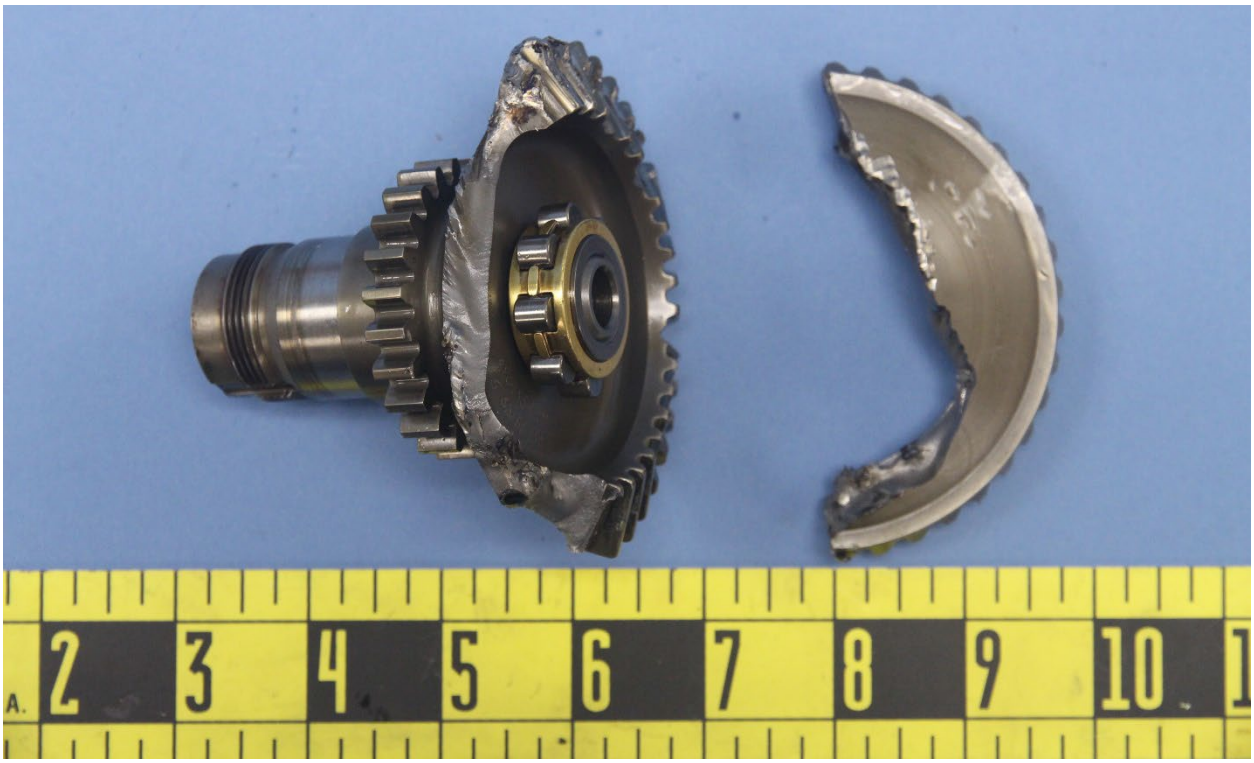

Figure 1. The largest gear fragments, as received.

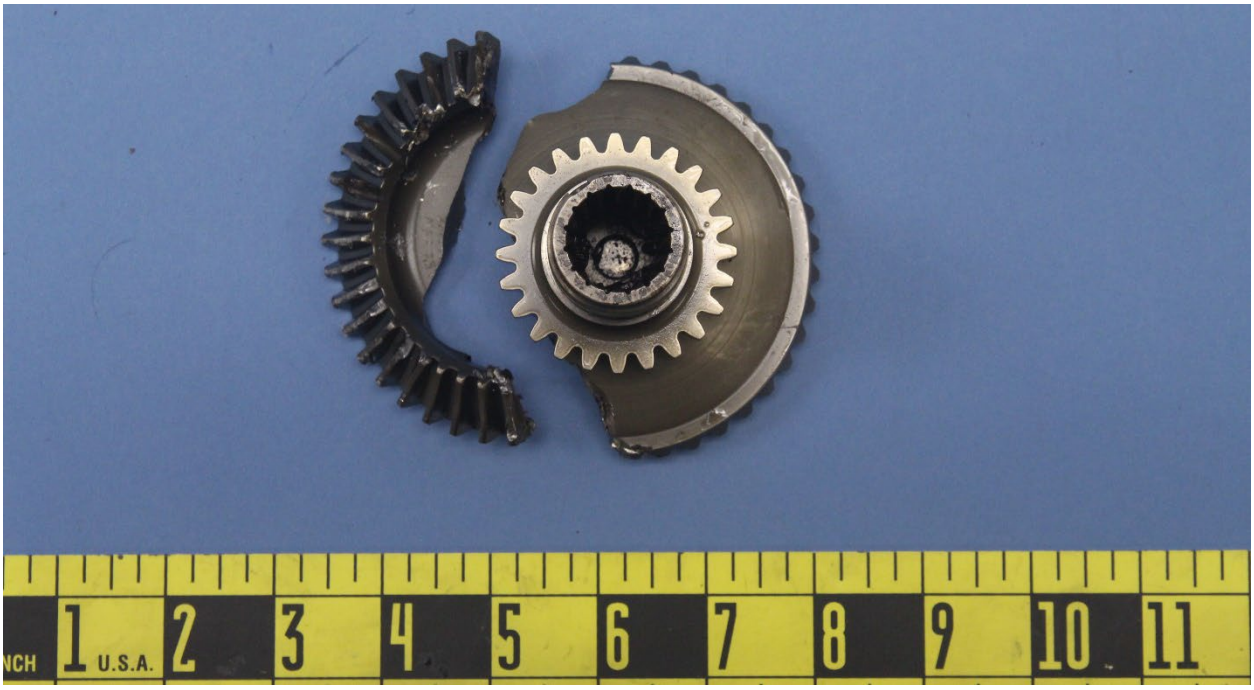

Figure 2. View of the mating fractured pieces, from the shaft side.

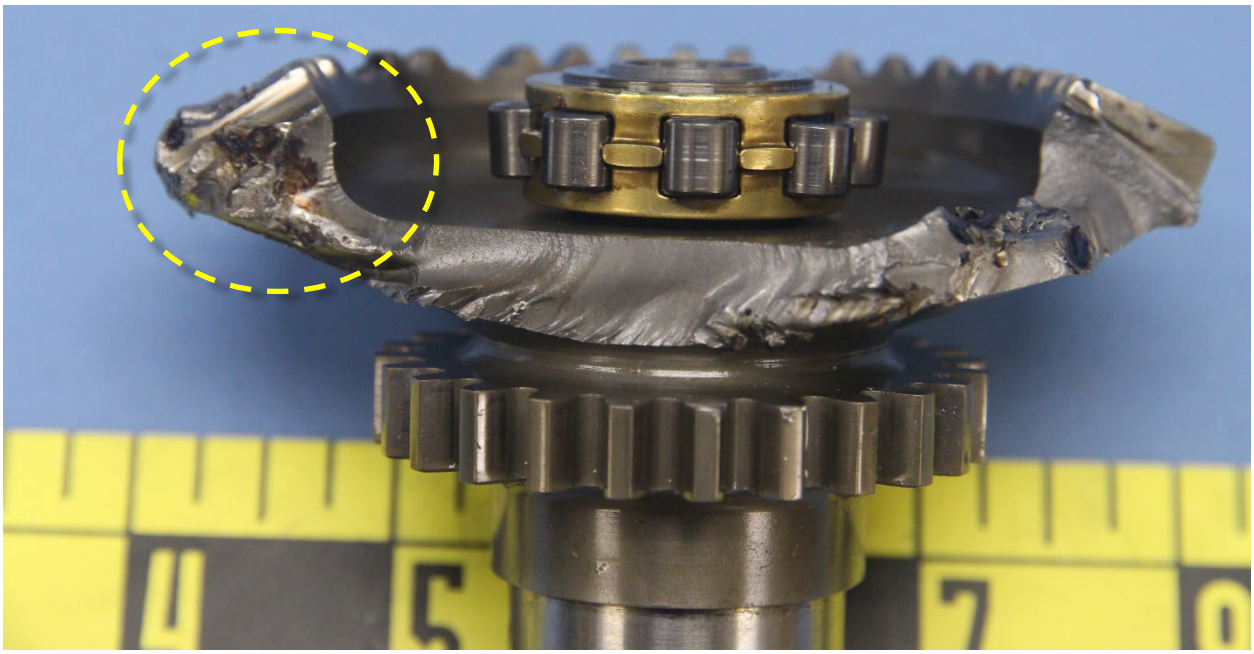

Figure 3. Closer view of the inboard mating main fracture surface of the gear. The circled area is highlighted in Figure 4.

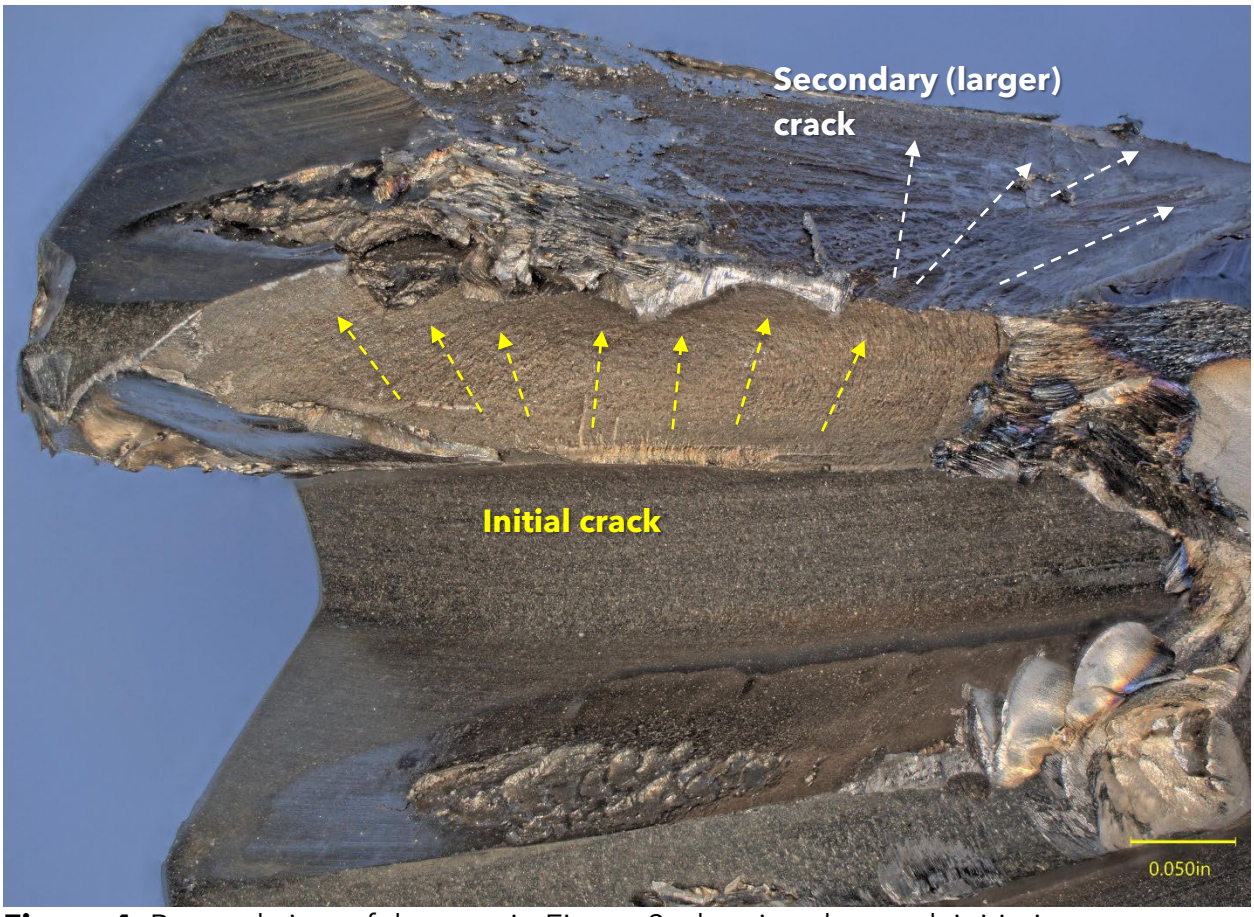

Figure 4. Rotated view of the area in Figure 3, showing the crack initiation area.

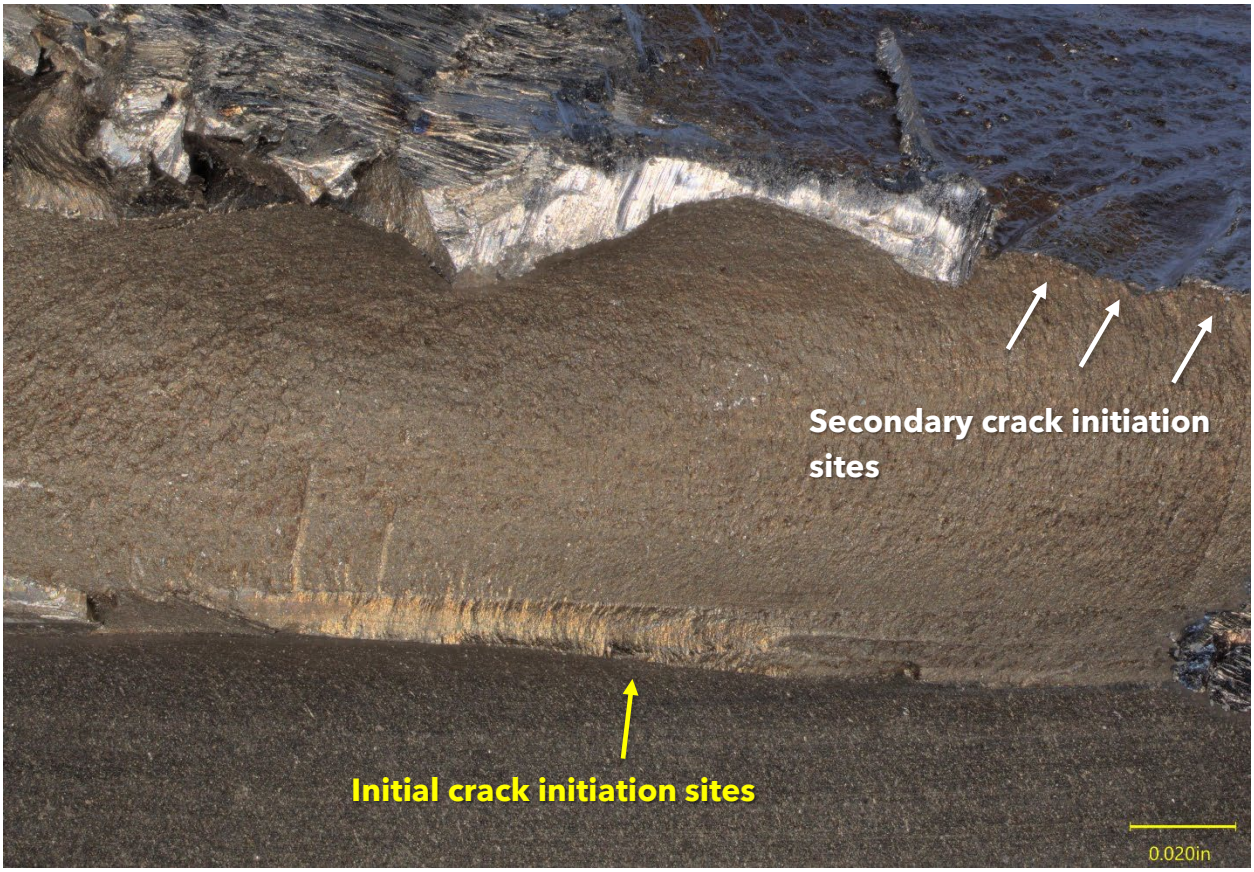

Figure 5. View of the initiation areas of the initial crack and the secondary crack.

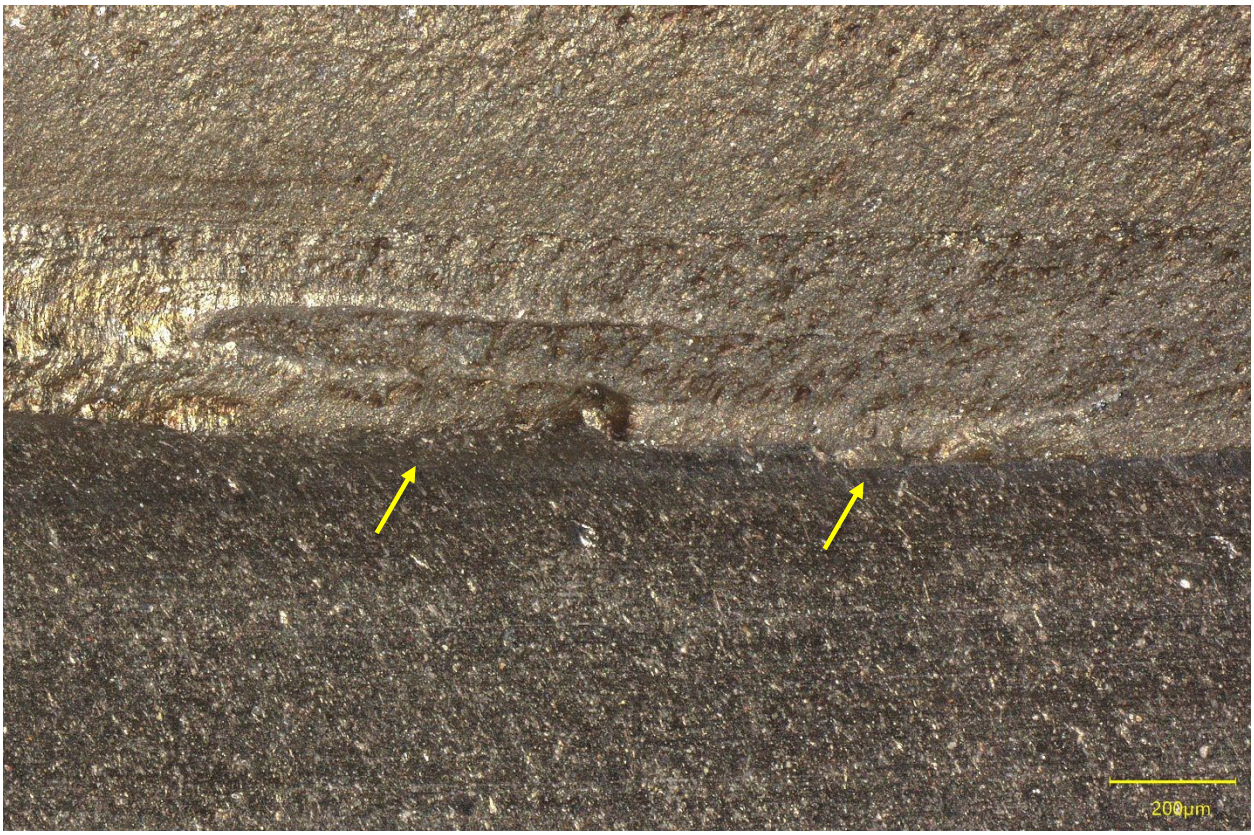

Figure 6. Closer view of the initial crack initiation sites (yellow arrows).

Figure 7. The initiation and initial propagation of the larger secondary crack.

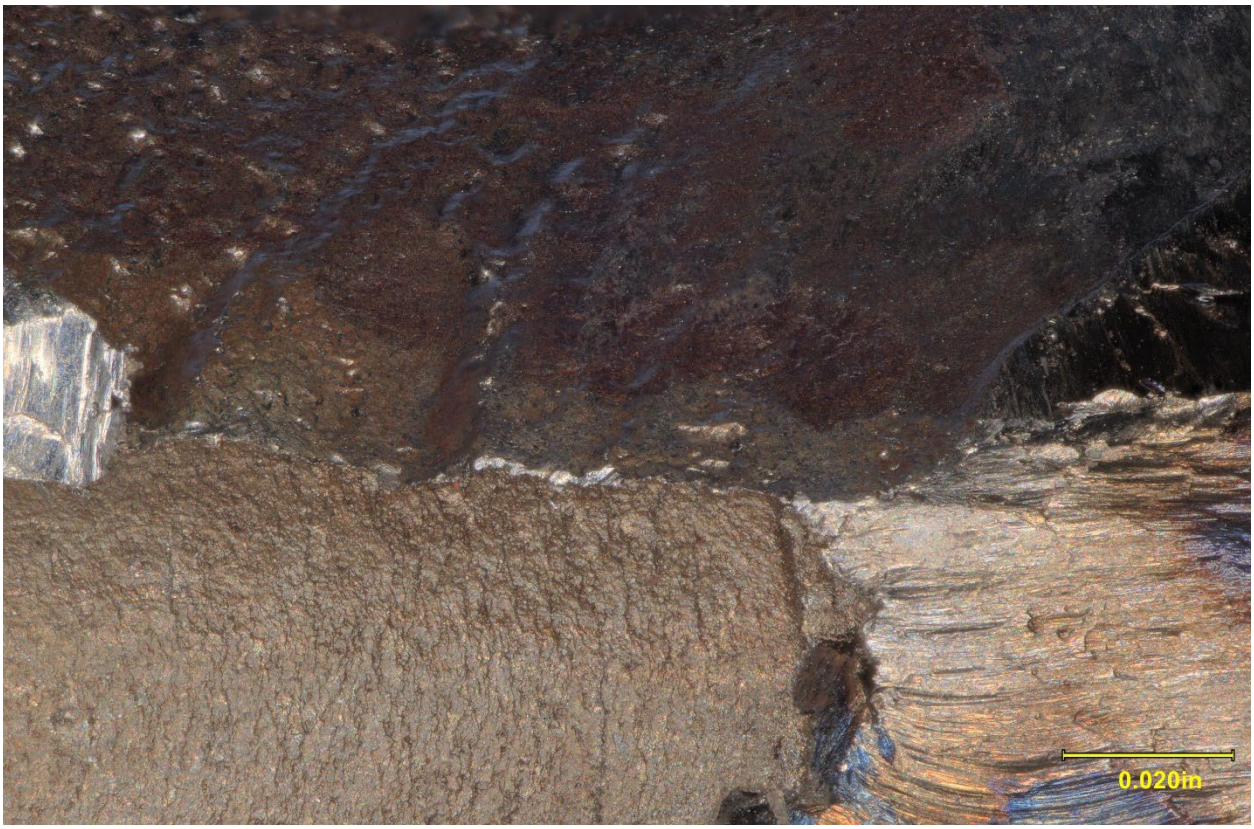

Figure 8. Closer view of the secondary crack initiation sites, originating from the initial fatigue crack.

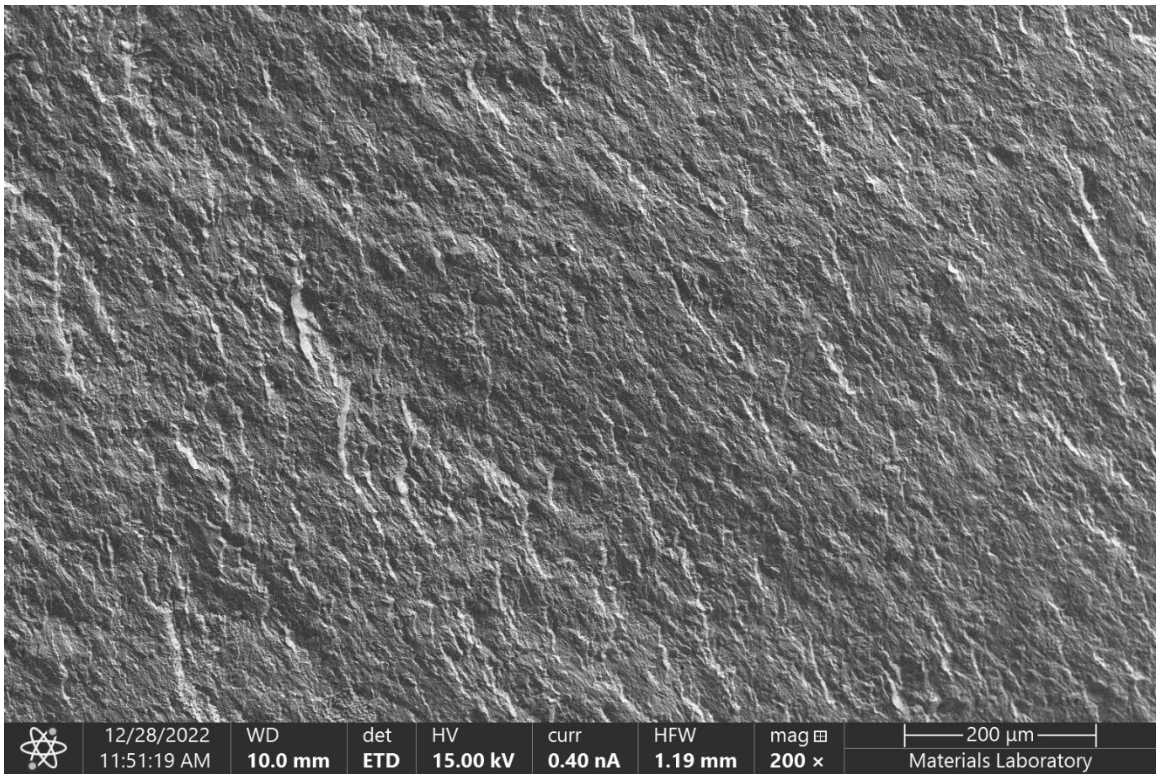

Figure 9. Secondary electron (SE) micrograph of a typical area of the larger fatigue crack.

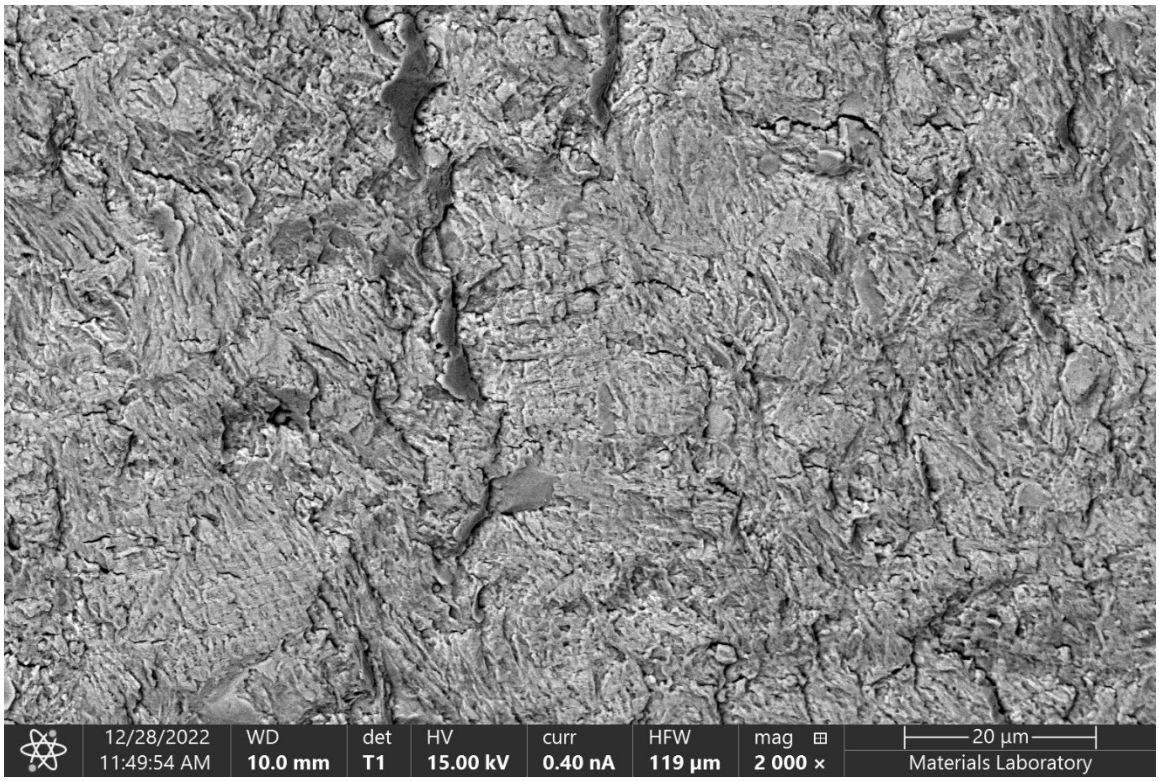

Figure 10. Backscattered electron (BE) micrograph of a the center of Figure 9.

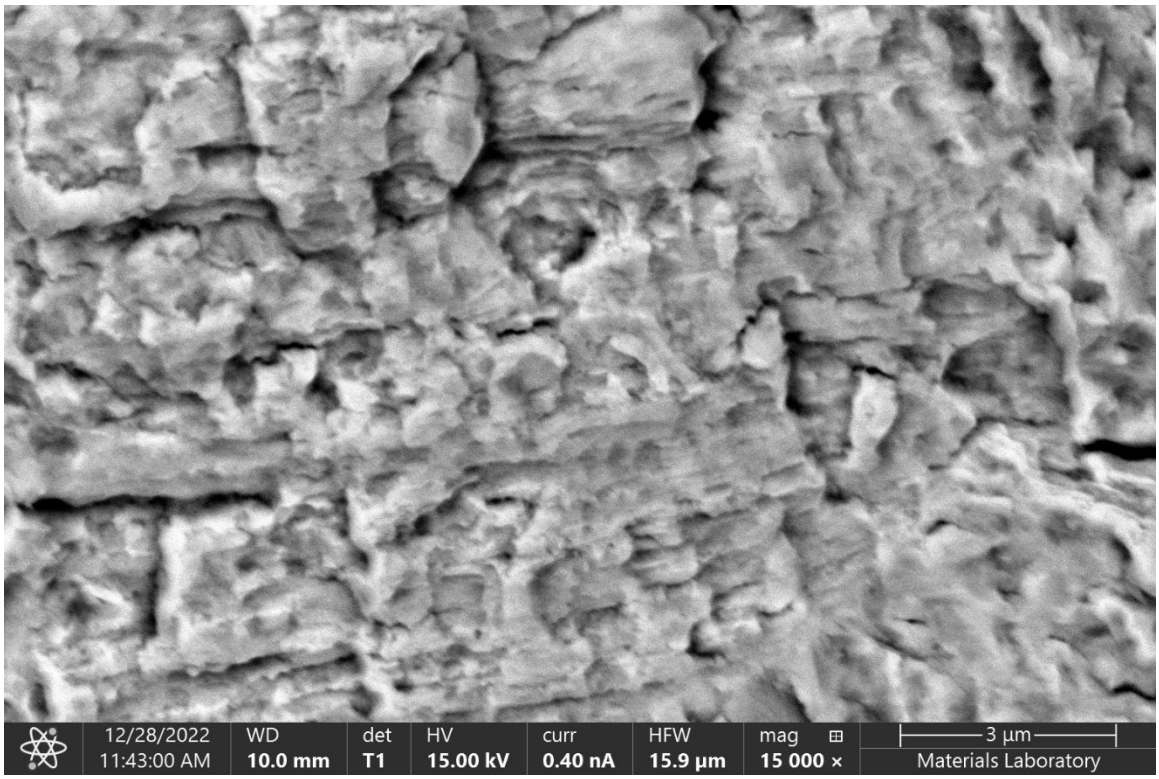

Figure 11. BE micrograph of fatigue striations from Figure 10.

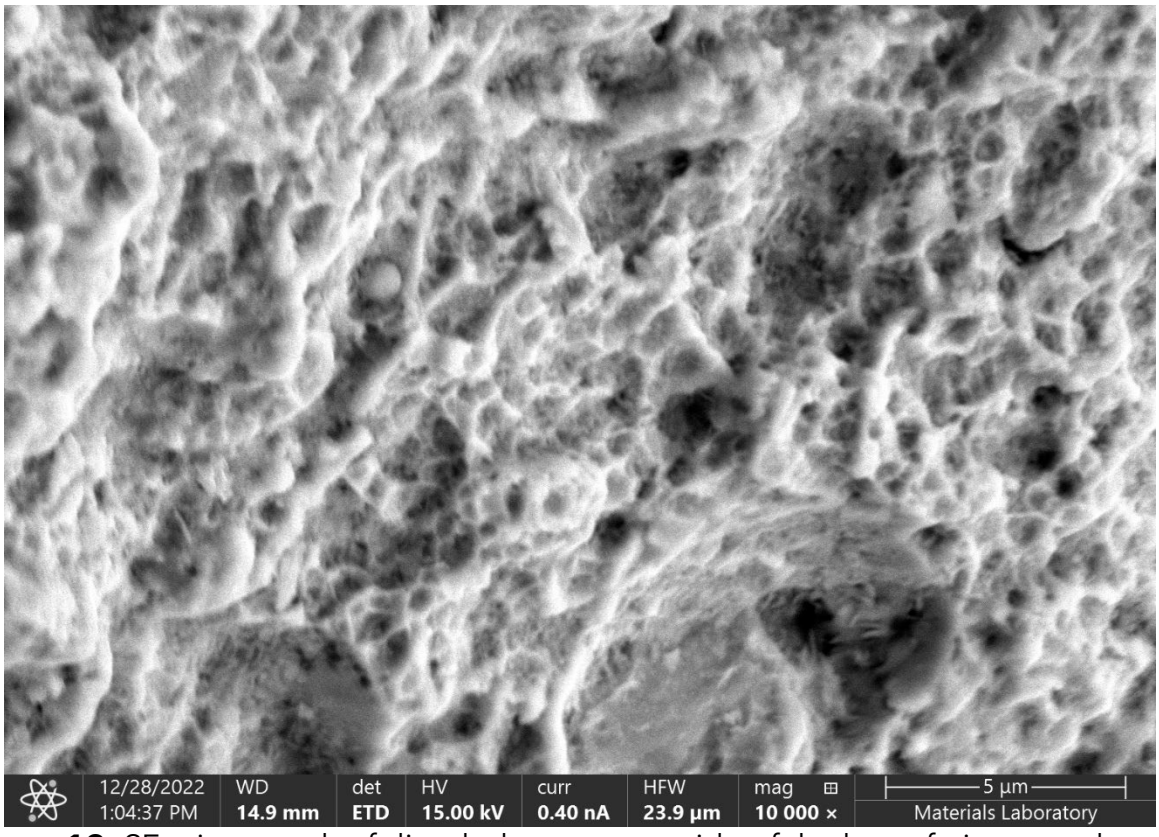

Figure 12. SE micrograph of dimpled rupture outside of the large fatigue crack.

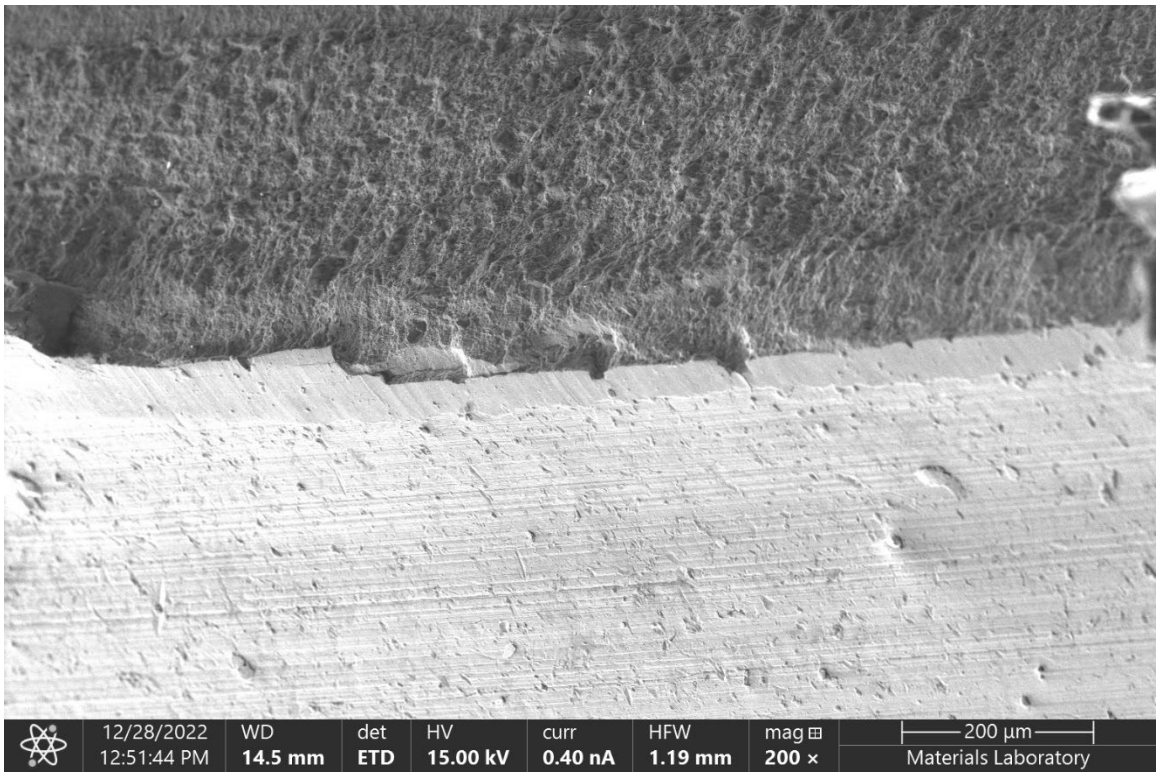

Figure 13. SE micrograph of initiation area of the initial fatigue crack.

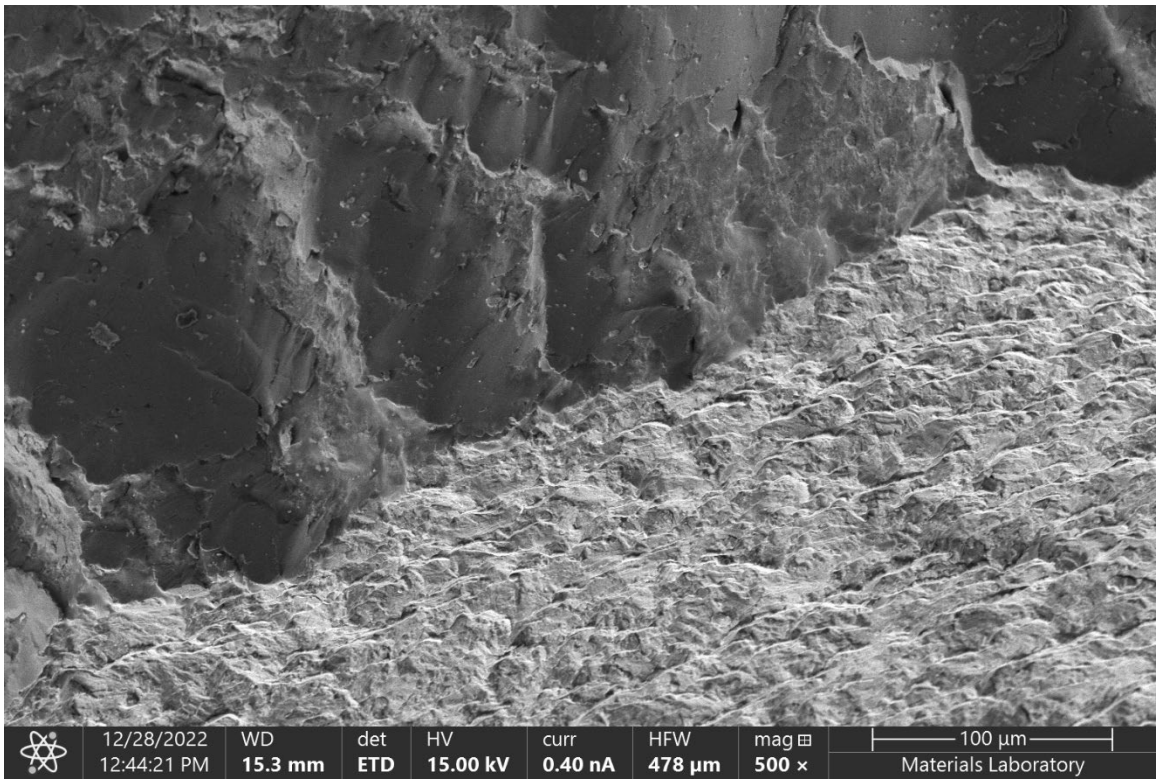

Figure 14. SE micrograph of the initiation sites of the secondary fatigue crack from the initial fatigue crack.

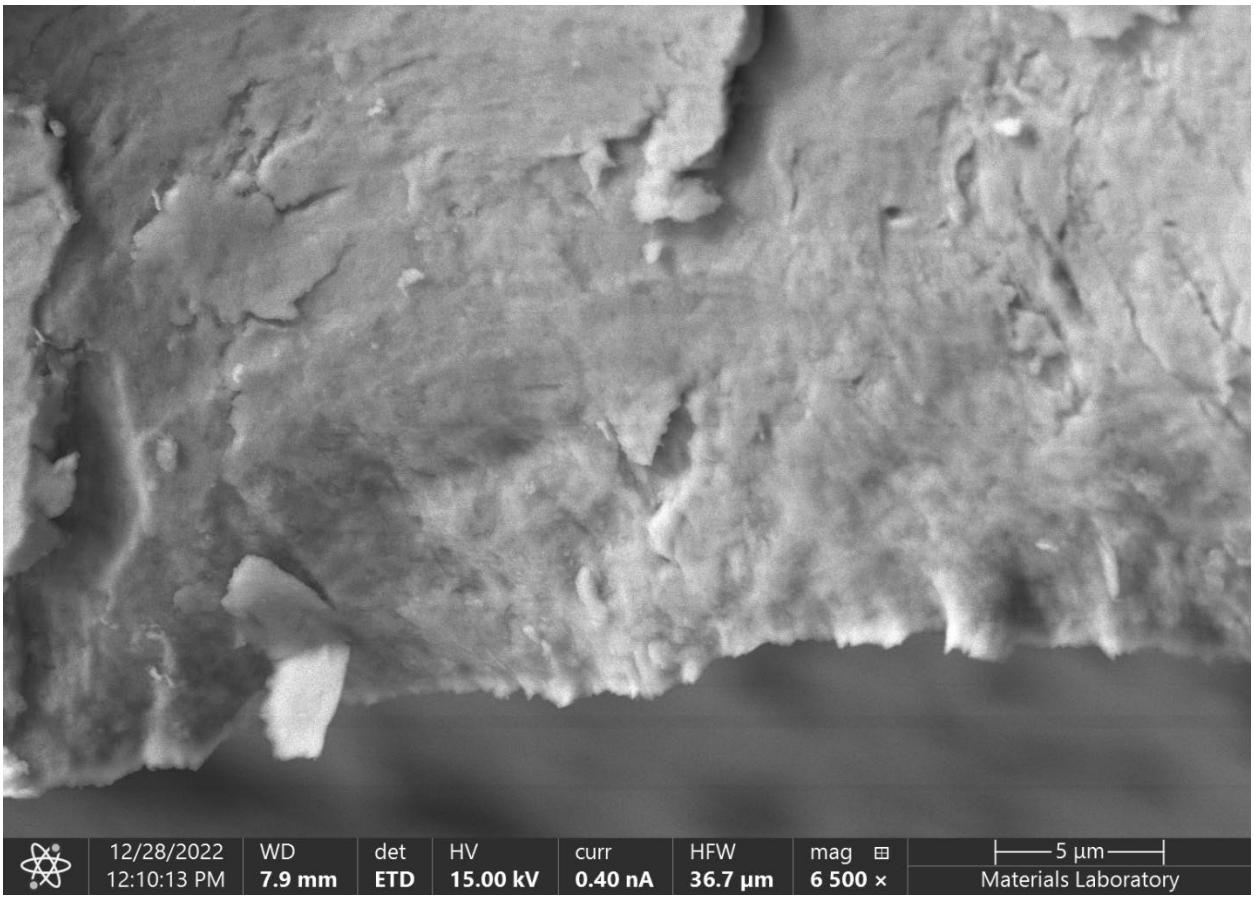

Figure 15. Closer view of the one of the initiation sites in Figure 14, showing striations propagating from the edge.

Figure 16. Another fatigue crack across a missing tooth on the gear.

Figure 17. Smaller fatigue cracks across a tooth of the gear, showing secondary cracking normal to the crack facing the reader.

Figure 18. View of a fatigue crack at a third missing tooth, showing adjacent damage to a land.

Figure 19. Bright-field (BF) electron micrograph of a cross section of the tooth near the main fatigue fracture (~50X, etched 2% Nital).

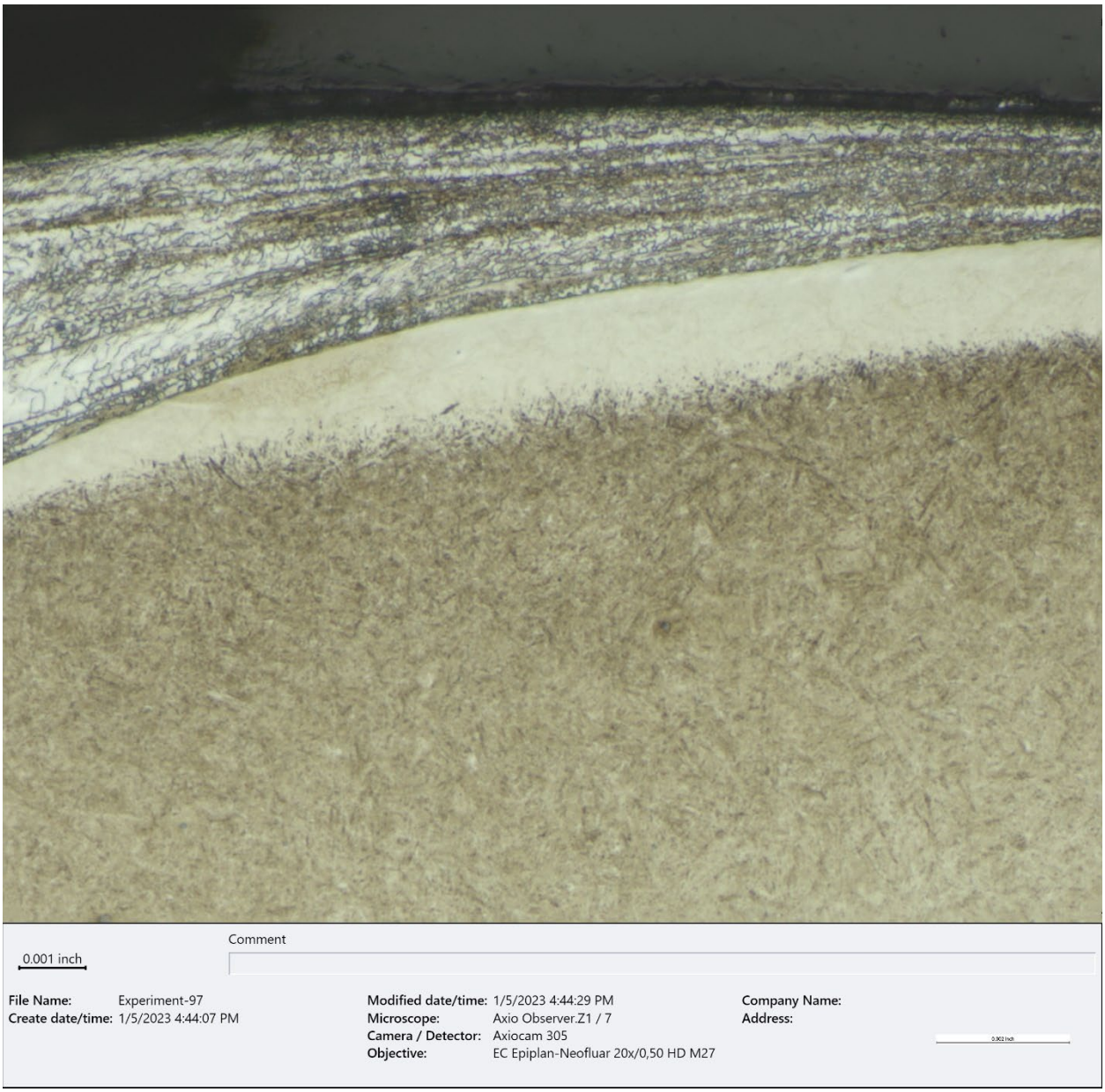

Figure 20. BF micrograph of the damaged top land of the gear thread in Figure 19 (~500X, etched 2% Nital).

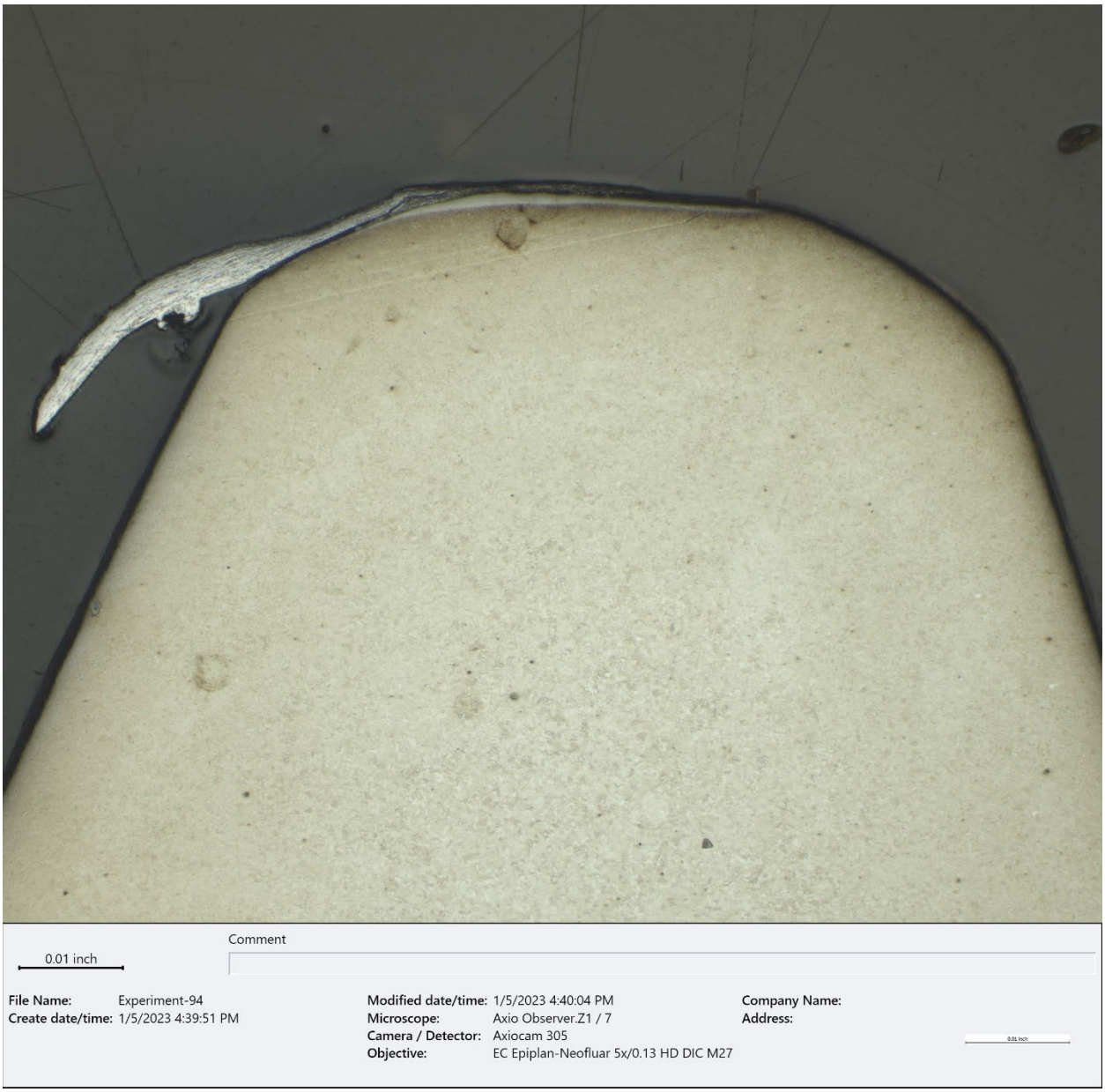

Figure 21. BF micrograph of a cross section of the tooth next to the one in Figure 19, showing deformed material and damage to the top land (~50X, etched 2% Nital).

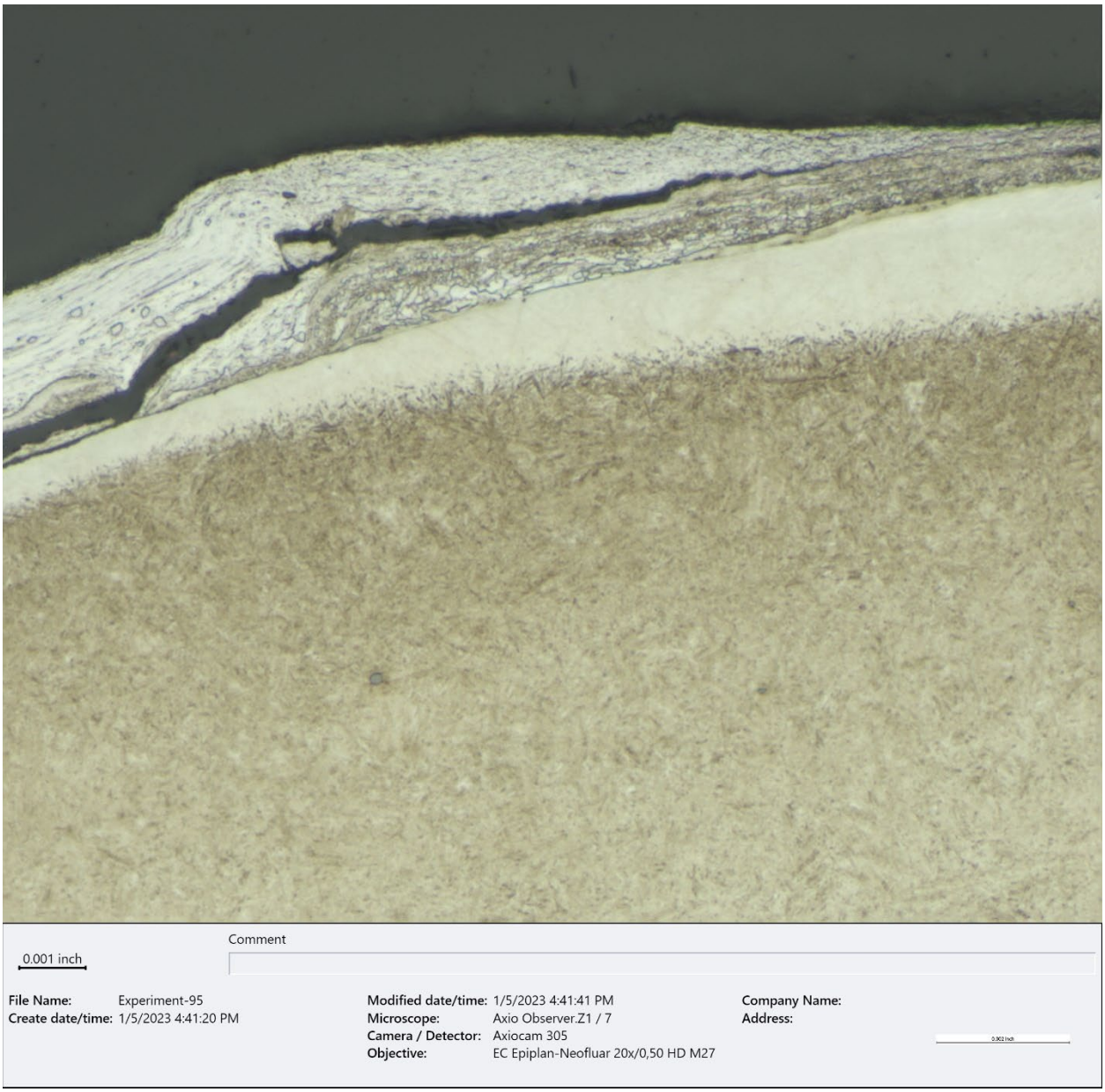

Figure 22. BF micrograph of a closer view of the tip in Figure 21, showing cracking in the deposited material on the top land (~500X, etched 2% Nital).

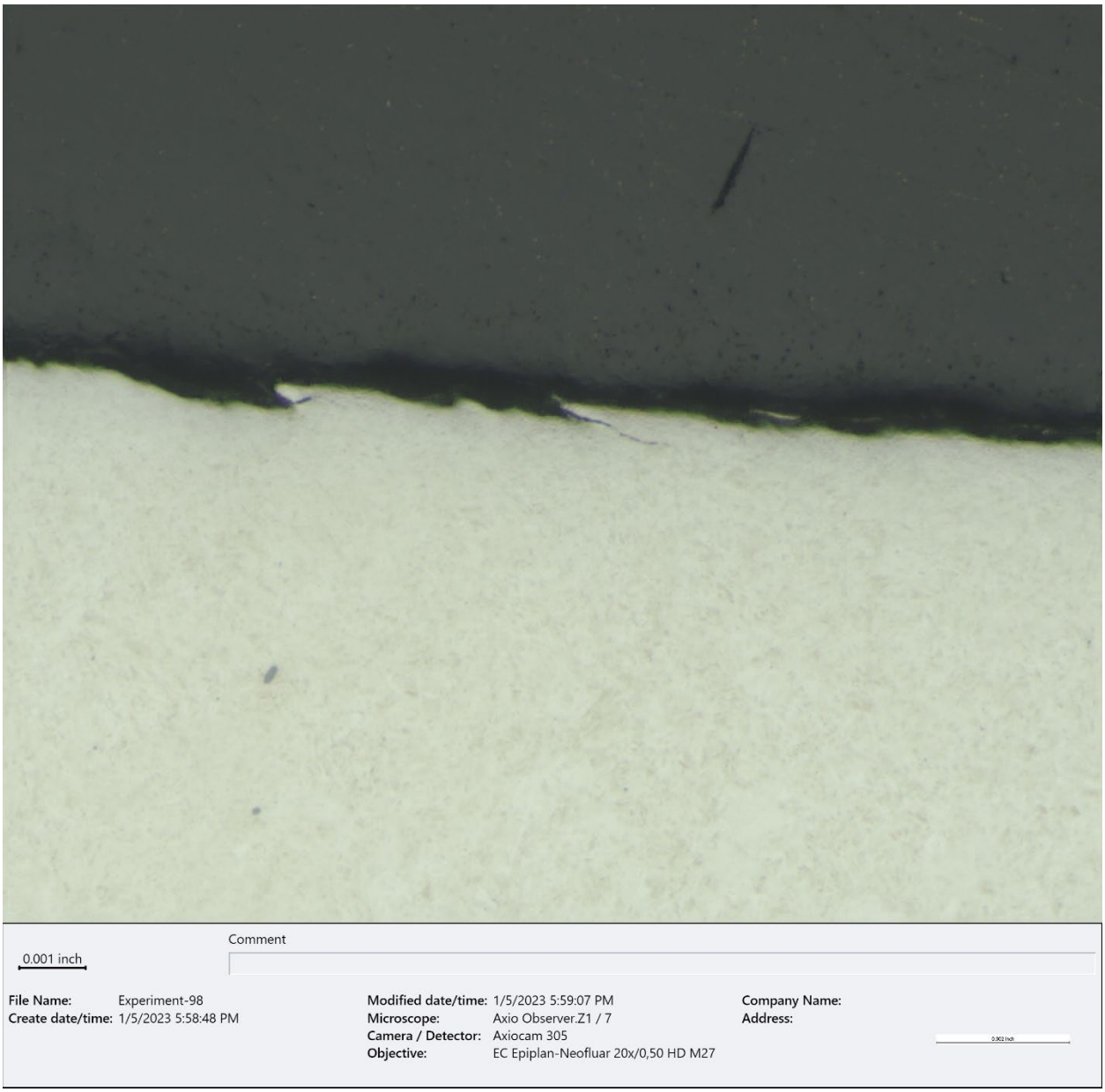

Figure 23. BF micrograph of small cracks from the worn and damaged areas of the flank, shown in Figure 4.

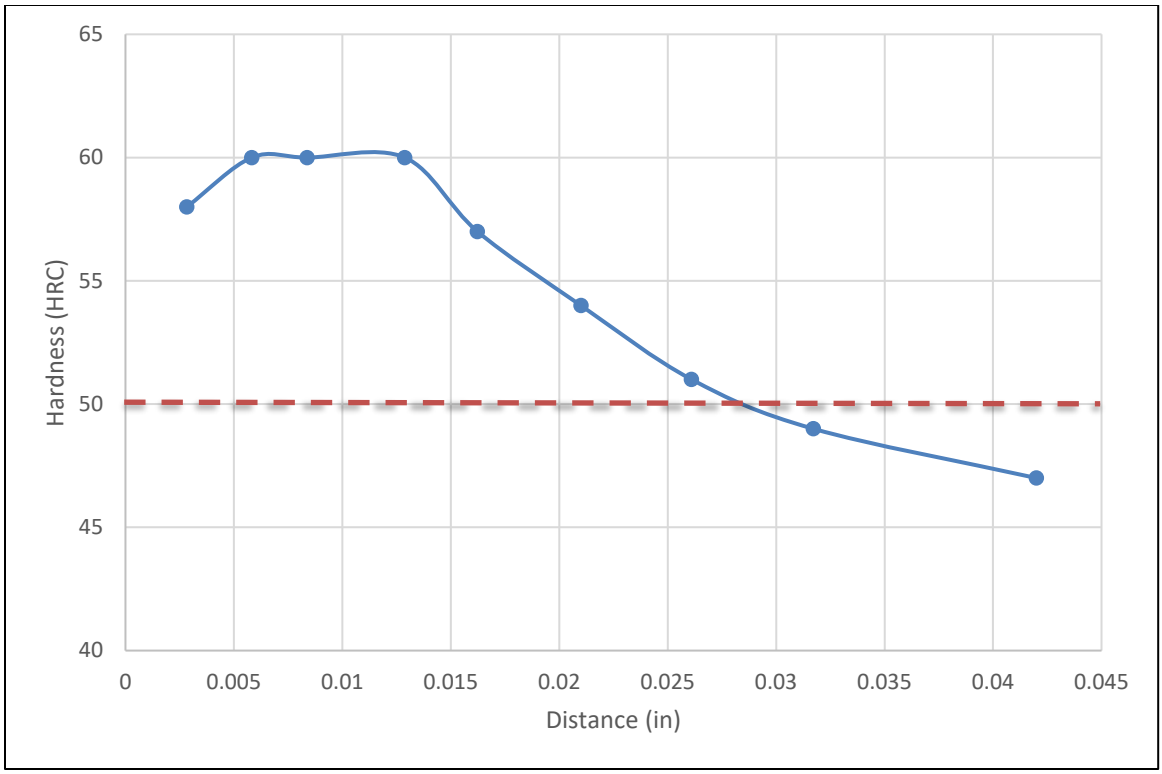

Figure 24. Chart plotting microindentation hardness data (in HRC converted from HK_{500}) versus the depth from the tooth surface. The dashed orange line represents 50 HRC, or the typical effective case depth hardness.